Kuwait Journal of Science 51 (2024) 100253

Contents lists available at ScienceDirect

Kuwait Journal of Science

journal homepage: www.sciencedirect.com/journal/kuwait-journal-of-science

Full Length Article

Cross-shelf transport of high chlorophyll-a coastal waters by frontal eddies in the south of Java sea

Mochamad Furqon Azis Ismail [a,b], Asep Sandra Budiman [a,*], Abdul Basit [a], Erma Yulihastin [a], Iis Sofiati [a], Subekti Mujiasih [a]

[a] Research Center for Climate and Atmosphere, National Research and Innovation Agency, Bandung, Indonesia
[b] GEOMAR Helmholtz Centre for Ocean Research Kiel, 24148, Kiel, Germany

ARTICLE INFO

Keywords:
Cross-shelf flux
Upwelling filament
Mesoscale eddies
Sea surface temperature (SST)
Chlorophyll-a

ABSTRACT

Intense mesoscale eddy activity has been observed off the southern Java coast (SJC), yet its impact on local ecosystems remains largely unknown. To investigate this, we examined remotely sensed altimetry, chlorophyll-a (Chl-a), and sea surface temperature (SST) data, focusing on their response to eddies in the region. Our eddy detection and tracking analysis revealed a unique cyclonic frontal eddy near the SJC coast and a large anticyclonic eddy offshore, active from July to September 2019. The cyclonic frontal eddy induced water transport through eddy filaments, upwelled subsurface cold water, and enhanced Chl-a concentrations by horizontally entraining Chl-a-rich shelf water offshore. The anticyclonic eddy then contributed to further distributing this enriched water southward. The mean cross-shelf transport associated with the frontal eddy was estimated at 1.80–2.33 Sv offshore, exporting approximately 1.87–2.40 $\times$ 10^3 tons of Chl-a to the Indian Ocean during its lifetime. Additionally, the spatial cross-correlation analysis of zonal and meridional wind stress with Chl-a revealed relatively high correlation values (0.6–1) and short lag times (<5 days) in offshore areas, indicating that the role of wind in the Chl-a advection cannot be ignored. We propose a three-stage mechanism to explain the presence of high Chl-a offshore:1) Wind-driven upwelling intensifies coastal nutrients, elevating Chl-a concentrations in coastal waters, 2) Frontal cyclonic eddy facilitates the retention and offshore export of these upwelling-enriched waters. and 3) Anticyclonic eddy advects these nutrient-rich waters further south. The combination of enhanced coastal upwelling and eddies can explain nutrient-rich coastal waters in offshore regions.

1. Introduction

Eddies have recently gained increased research focus due to their significant roles in oceanic processes, including mass transport (Ismail et al., 2017), heat transfer, larval dispersal (Harrison et al., 2013), and chlorophyll-a (Chl-a) distribution. Numerous studies have revealed how cyclonic eddies (CE) can enhance biological and biogeochemical activity by uplifting nutrients to the euphotic zone, while anticyclonic eddies (ACE) tend to suppress local productivity (McGillicuddy, 2016; Pessini et al., 2018). Notably, Cordeiro et al. (2015) observed that equatorward jet-related instabilities within upwelling systems frequently manifest as meanders, eddies, and filaments.

Upwelling filaments are long (100–200 km), have narrow sections (10–50 km), and are cold-water structures that extend from the coast to the oceanic region. They play a crucial role in transporting water containing nutrients and Chl-a (Álvarez-Salgado et al., 2001), as well as distributing eggs and larvae of several marine species from the coastal zone to the open ocean (Harrison et al., 2013; Rodriguez et al., 1999). Filaments can be easily recognized in remote sensing images due to their strong sea surface temperature (SST) and Chl-a signatures (Marcello et al., 2005; Smyth et al., 2001; Vipin et al., 2015) or by direct measurement of water velocity (Cravo et al., 2010; Shapiro et al., 2010). Chl-a is a proxy for phytoplankton biomass, which is an indicator of nutrient availability in the water column, while SST is a measure of the temperature of the water (Alvarez et al., 2012). Vipin et al. (2015) stated that gradients in water properties are observed at the edges of filaments, and these gradients are often so high that the edges form fronts. In addition, there are numerous methods for approximating the filament's width. Ribbe et al. (2018) used a maximum horizontal gradient of SST and Chl-a while identifying a filament off the coast of eastern Australia.

* Corresponding author.
E-mail address: assandra036@brin.go.id (A.S. Budiman).

https://doi.org/10.1016/j.kjs.2024.100253
Received 11 April 2023; Received in revised form 9 May 2024; Accepted 22 May 2024
Available online 23 May 2024

García-Muñoz et al. (2004) evaluated the transport in the NW Africa coastal transition zone region by using a section that crossed the filament along a certain longitude and latitude. Vazquez-Cuervo et al. (2017) identified upwelling off Peru and Chile by finding maximum SST gradients in the 0.03 ± 0.02 °C km^{-1}. Cordeiro et al. (2015) located upwelling filaments in an Iberian Peninsula numerical simulation manually by using a threshold value of 0.075 °C km^{-1}, and Artal et al. (2018) detected and characterized upwelling filaments in a numerical ocean model by using a threshold of 0.07–0.10 °C km^{-1}. It should be noted that other processes such as rainfall and river discharges can also impact SST and Chl-a concentrations along the coast (Navarro and Ruiz, 2006; Santos and Ribeiro, 2005; Chinacalle-Martínez et al., 2021), which in turn, will influence the determination's result.

The anatomy or vertical structure of the filament can be better investigated with data of current, Chl-a, and SST at a certain depth, which can only be obtained through direct measurements. The availability of these data will make the study of filaments more accurate than relying solely on remote sensing data (Navarro-Olache et al., 2004; Shapiro et al., 2010). However, because the filament is an upper-layer structure that barely exceeds the top 150 m (Cravo et al., 2010), the determination of the filament's thickness based on this depth can be considered. The southern region of Java is a dynamic region in the southern region of the Indonesian Maritime Continent (Fig. 1a), characterized by an eddy hotspot area (Ismail et al., 2021). Moreover, the south of Java is frequently occupied with locally generated eddies (Feng and Wijffels, 2002; Yu and Potemra, 2006) that contribute to offshore export transport of high biological productivity (Iskandar et al., 2010; Ismail et al., 2021; Yang et al., 2019). The southern region of Java is widely known as a seasonal upwelling system in the eastern boundary region, which peaks in July and August (Horii et al., 2018; Wirasatriya et al., 2020; Budiman et al., 2022). Yang et al. (2019) suggested that high Chl-a (>0.2 mg m^{-3}) exists within 200 km off the Java coast and is spread over 1000 km offshore during the upwelling season. Meanwhile, Peliz et al. (2004) found the maximum Chl-a background of 0.2 mg m^{-3} while studying the upwelling filament southwest of Iberia in the winter of 2001. In the south of Java waters, high Chl-a and cold SST are often distributed far offshore due to the mesoscale eddies (Fig. 1b and c). According to (Iskandar et al., 2010), offshore Chl-a blooms in the southeastern tropical Indian Ocean, particularly in the south of Java during boreal summer-fall 2006, are strongly related to high eddy kinetic energy.

Cross-shelf circulation caused by mesoscale features such as eddies and filaments is frequently identified as the primary mechanism of shelf-deep seawater exchanges (Bassin et al., 2005). Further, Bassin et al. (2005) suggested that coastal eddies impact nutrient supply and organic matter export with a diameter of 4–15 km and a lifespan of 2–6 days. Eddies with these characteristics are categorized as small-scale eddies based on Lian et al. (2019), who suggested that mesoscale eddies in the ocean are characterized by swirling currents with a horizontal spatial size of 10^1–10^2 km and a temporal scale of 10^1–10^2 days. Although several studies on eddies in this area have been carried out (e.g., Iskandar et al., 2010; Yang et al., 2019; Ismail et al., 2021), little is known about the role of eddies in cross-shelf water mass exchanges in the region. Peliz et al. (2004) computed cross-shelf eddy-induced transport caused by a substantial eddy filament reaching the shelf southwest of the Iberian Peninsula. By applying a similar method, Shapiro et al. (2010) estimated the transport of water induced by an individual mesoscale eddy off the northwest coast of the Black Sea. Jiaxun et al. (2017) used approximated filament width and jet depth values to document a considerable offshore filament-induced transport. Ribbe et al. (2018) derived the cross-shelf volume transports associated with eddy filaments along a western boundary current off Southeast Queensland, Australia. Here, the offshore transport of Chl-a-rich water filament is quantified for the first time in the transitional zone south of Java. These studies provide evidence that eddies play a crucial role in the distribution of high chlorophyll-a and cold SST far offshore in the

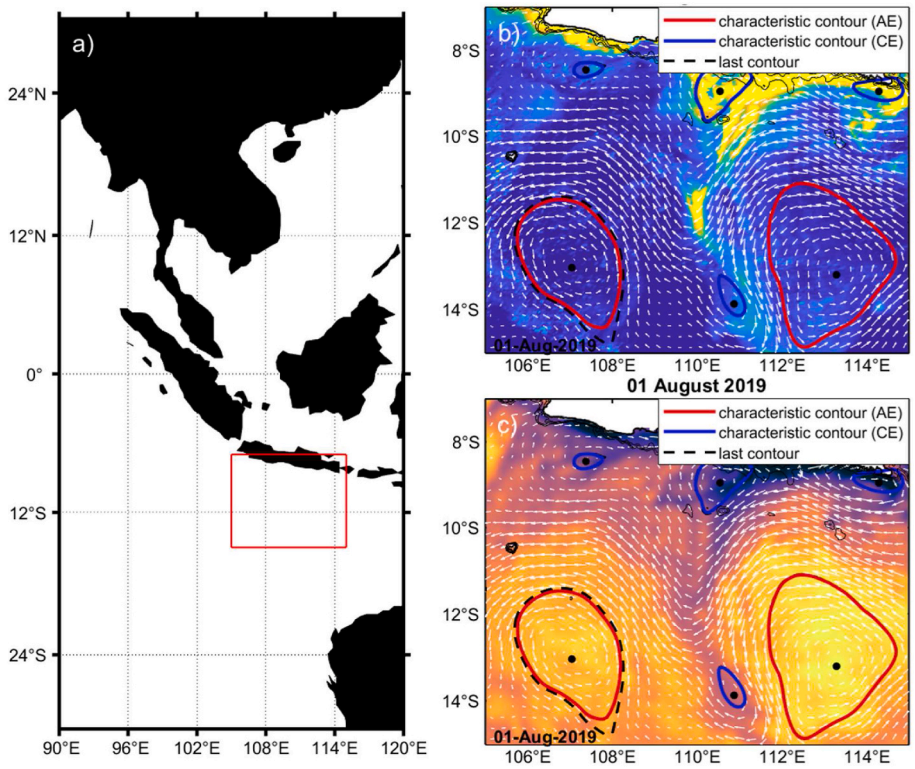

Fig. 1. The study domain in the Southeastern Indian Ocean region (red rectangle in a) with a snapshot of Chl-a (b, units in mg m^{-3}) and SST (c, units in °C) on 1 August 2019 with the presence of cyclonic (CE) and anticyclonic eddies (ACE). White vectors mark the geostrophic currents. (For interpretation of the references to colour in this figure legend, the reader is referred to the Web version of this article.)

waters south of Java. Their ability to transport nutrients and water masses makes them important drivers of primary productivity and ocean circulation in the region. According to our study domain, Yang et al. (2015) found that eddies were responsible for up to 50% of the chlorophyll-a variability in the region. The study also found that eddies were more likely to occur during the upwelling season (June to September) when winds drive nutrient-rich water to the surface. Hatmaja et al. (2023) suggested that during the upwelling season coinciding with the peak of positive Indian Ocean Dipole (IOD), the increased number and strength of cyclonic eddies contribute significantly to colder sea surface temperature anomalies and higher chlorophyll levels.

In this study, we explored the roles of cyclonic and anticyclonic eddies in distributing chlorophyll-a (Chl-a) offshore in the south of Java during the peak of the 2019 South Java upwelling event. Among several eddies observed, cyclonic eddy C1 and anticyclonic eddy A6 emerged as dominant influences, transporting nutrient-rich water masses further offshore. Eddy C1 traveled near the shelf area, while eddy A6 propagated further offshore. Meanwhile, we assessed the southeasterly wind as the background conditions to have a comprehensive analysis result in determining the coupled forcing that induced Chl-a distribution offshore. This research contributes valuable insights into the mechanism of the Chl-a's presence offshore in the south of Java while highlighting the potential impacts of eddies on Chl-a's distribution and nutrient transport.

The paper aims to calculate Chl-a rich water filament flux by the mesoscale eddies that traveled along the SJC from 10 July to 25 August 2019 using satellite-derived Chl-a, sea surface height anomaly (SSHA), and SST. We focus on the conditions on 21 August 2019, when a cyclonic eddy near the shelf area coincident with the anticyclonic eddy offshore in the south of Java waters, converging with the Chl-a rich water due to an upwelling event at that time (Lumban-Gaol et al., 2021). In the middle of the two targeted eddies propagation on 1 August 2019, the SST and Chl-a snapshot shows an intense front around 700 km long and 60-70 km wide was seen to be transported offshore from the shelf (Fig. 1b and c). The findings of this study will contribute to a better understanding of the dynamics and impacts of eddies in the region, providing valuable insights for resource management and marine conservation efforts.

However, the wind-induced upwelling cannot be ignored as another factor influencing the Chl-a filament distribution in the south of Java waters. Yang et al. (2019) have shown that the background conditions, including the wind, manifested in the form of upwelling and non-upwelling seasons, have an essential role in eddy-induced Chl-a distribution. The wind can increase the vertical shear of the background currents, which can promote energetic eddies (Yang et al., 2019; Akpinar et al., 2022). Meanwhile, Hanifah et al. (2016) demonstrated that the formation of eddies in the south of Java is influenced by the shear velocity generated by several current systems rather than by local winds. Rubio et al. (2018) proposed that winds enhance coastal upwelling, while the subsequent formation of eddy facilitated the offshore export and retention of the upwelling enriched waters. Therefore, to better understand Chl-a filament distribution offshore, we continue our analysis to assess the role of the local wind.

2. Material and methods

2.1. Data

We use daily merged satellite altimetry multimission data, including SSHA and geostrophic surface currents from January 2019 to December 2019 for the south of Java waters region (105-115°E, 7–15°S). These data are provided by the E.U. Copernicus Marine Environment Monitoring Service (last visited April 2021) and available at a spatial resolution of 0.25° (approximately 25 km) in latitude and longitude and were collected during the following satellite altimetry missions: Jason-1/2/3, Sentinel-3A, HY-2A, Saral/Altika, Cryosat-2, ERS1/2, TOPEX/Poseidon, ENVISAT, GFO, and ERS1/2.

Chl-a data obtained from Global Ocean Colour (Copernicus-GlobColour), Bio-Geo-Chemical, L4 (monthly and interpolated) from Satellite Observations (1997 - ongoing), Product Id: OCEANCOLOUR_GLO_BGC_L4_MY_009_104 (last visited April 2021). The 4 km x 4 km daily charts of Chl-a concentration were selected between July and September 2019 to focus on the filament event.

Daily wind data was retrieved from ERA5 with a spatial resolution of 25 km x 25 km.

2.2. AMEDA algorithm for eddy tracking

We employ Angular Momentum Eddy Detection and Tracking Algorithm (AMEDA) to identify and track eddies (Le Vu et al., 2018). AMEDA is a hybrid detection method based on physical parameters and the geometrical properties of the velocity field. All the closed streamlines surrounding the selected eddy center were located to determine each eddy characteristic, such as R_{max}, Vel_{max}, and Kinetic Energi (KE). Rmax represents the maximum radius of the eddy, defined as the largest distance from the eddy center to any point on the eddy's boundary. R_{max}, Vel_{max}, and KE defined as follows:

$$R_{max} = \max\left(\sqrt{(x - x_c)^2 - (y - y_c)^2}\right) \ldots \quad (1)$$

$$Vel_{max} = max\left(\sqrt{u^2 + v^2}\right) \ldots \quad (2)$$

$$KE = \frac{1}{2}\rho \sum_{i=1}^{n} (u^2 + v^2) dA \ldots \quad (3)$$

Where x and y are the coordinates of a point on the eddy's boundary. x_c and y_c are the coordinates of the eddy center. u and v are the zonal and meridional components of the velocity vector at a point within the eddy. ρ is the density of water dA is the area of a small region within the eddy. The amount of filament transported through the eddy-induced jet offshore was computed using the following equation (Shapiro et al., 2010).

$$T = v.w.d \ldots \quad (4)$$

where T is the transported upwelling filament by a frontal eddy (Sv), v is the surface geostrophic current velocity inside the eddy (m s^{-1}), w is the width of filament (m), and d is the depth or thickness of the filament (m). Peliz et al. (2004) defined d as the shelf break depth to estimate the cross-shelf transport induced by eddy interactions.

The width of the filament w defined by applying a Chl-a horizontal gradient threshold of 0.2 mg m^{-3} km^{-1} across the filament at the same latitude. A Chl-a threshold value of 0.2 mg m^{-3} was considered based on Yang et al. (2019). The absolute horizontal gradient of the Chl-a concentration C is calculated according to Ribbe et al. (2018) as follows:

$$|\vec{\nabla} C| = \sqrt{\left(\frac{\partial C}{\partial x}\right)^2 + \left(\frac{\partial C}{\partial y}\right)^2} \ldots \quad (5)$$

Where $\nabla = \left(\frac{\partial}{\partial x}, \frac{\partial}{\partial y}\right)$ is the gradient operator, and x and y are the zonal and meridional coordinates.

The horizontal gradient threshold is also applied in determining the filament width based on SST. A threshold value of 0.15 °C km^{-1} was chosen based on the range generated by Barbieri et al. (1995). To better understand the possibility of another force or contributor in distributing Chl-a offshore in the south of Java, winds were analyzed during the peak period of upwelling (July to August) and were cross-correlated with Chl-a.

3. Results

3.1. Characteristics and dynamics of the targeted eddy

Several eddies were observed during the peak period of the South Java upwelling event in 2019 (July–August), causing them to move cold and nutrient-rich surface waters. Among all, cyclonic eddy C1 and anticyclonic eddy A6 were observed to have a dominant influence in distributing filaments containing cold and nutrient-rich water masses further offshore. Cyclonic eddies C1 traveled near the shelf area south of Java (Fig. 2a). This eddy first appeared on 13 July 2019, about 50 km offshore, then moved northwestward and gradually got closer to the shelf edge at the end of its track. During its propagation, its physical properties, such as the maximum azimuthal velocity (Vel_{max}), the maximum radius (R_{max}), and the kinetic energy (KE) fluctuated along with its track but generally tended to show an increase in value from its starting point (Fig. 2b, c, and 2d). Vel_{max}, R_{max}, and KE have a mean value of 0.27 ± 0.08 m s^{-1}, 50.24 ± 16.67 km, and 4.04 ± 2.87 m^2 s^{-2}, respectively. Vel_{max} reaches its peak on day 44 (24 August 2019) with a maximum value of 0.46 m s^{-1} as well as the maximum value of Kinetic Energy (KE) of 10.67 m^2 s^{-2} (Fig. 2b and d).

Meanwhile, the targeted anticyclonic A6 propagated offshore at a latitude between 12 and 14°S for 53 days from 22 July 2019 to 13 September 2019 (Fig. 2a). Vel_{max}, R_{max}, and KE have a mean value of 0.35 ± 0.21 m s^{-1}, 109.9 ± 71.28 km, and 56.61 ± 60.59 m^2 s^{-2}, respectively. At the beginning of its propagation, Vel_{max} increased gradually from about 0.3 m s^{-1} on 22 July 2019 to 0.7 m s^{-1} on 6 August 2019, while R_{max} And KE increased gradually from about 25 km to 0.03 kg m^2 s^{-2} to 200 km and 175 m^2 s^{-2}, respectively (Fig. 2e, f, and 2g). Vel_{max} became steady until day 30th and then decreased to about 0.1 m/s on average until it dissipated (Fig. 2e). R_{max} decreased smoothly from 200 km on day 15th to about 140 km on day 30th of propagation, while KE fell more sharply from 175 kg m^{2}s^{-2} to 75 kg m^{2}s^{-2} during that period. In the remainder of its propagation, all physical properties (Vel_{max}, R_{max}, and KE) were weakened to about <0.2 m s^2, <50 km, and <50 kg m^2 s^{-2}, respectively. A6, with a longer lifespan of 53 days, allowed for more time to interact with the geostrophic current and potentially merge with smaller eddies, contributing to its observed growth and intensification. This suggests that A6 might have access to more energy sources than C1.

In general, all eddies' characteristic signals move in line. The peak KE signal always coincides with the peak radius signal in the speed range, which is still relatively high, both in CE and ACE eddy. That is why the anticyclonic eddy's KE has a greater value than the cyclonic eddy's KE due to the larger size or radius.

3.2. Dynamics of upwelling filaments

On 10 July 2019, the day the targeted eddy appeared (C1 in Fig. 3), there were at least 6 other CE and 4 ACE in the study area. A filament formed at about 10–12°S with a tongue sticking out among the eddies C3, C5, A1, and A5. The source of this filament was from the southern coast of Java with a longitude east of 115°E and was distributed further west until it reached a longitude of 108°E by those eddies. Fig. 3a clearly shows how the filament formation was formed by nearby eddies. Two weeks later, on 24 July 2019, the surviving eddies in the study area were C1, C4, and A5 (Fig. 3b). C1 formed a relatively wide (100 km) filament with a tongue extending to latitude 14°S.

A cyclonic eddy C4 on the east side of C1 is now closer to the coast and has formed another filament. A closer look shows that the filaments with lower Chl-a concentration (0.3 mg m^{-3}) were distributed westward at 106°E and 10°S and formed arcs following the eddy perimeter of the anticyclone A5. We can even see a high concentration of Chl-a in the southwest corner of the A5 edge, which is thought to be an accumulation of these filaments. After two weeks of formation, filaments were further expanded with A6 and C9 (Fig. 3c). The filaments are distributed further south along the large perimeter of A6 which is about 200 km, until 15°S and appear to bulge at 12°S. C5 spreads filaments further south to latitudes greater than 15°S. Meanwhile, C8 emerges as new cyclonic eddies on the west side of C1, at a position around 107°-108°E and 8°-9°S, and distributes Chl-a around its perimeter, forming a ring-shaped filament there. C4 is still on the east side of C1 with filaments around its edge but now extends south to 11°S. Chl-a filaments with a concentration of 0.7–0.8 mg m^{-3} seemed to accumulate in the southernmost part of the filament. A5 has a smaller diameter (80 km) further west (106° E) than before (120 km, 108.25°E). It carries Chl-a filaments sourced from the

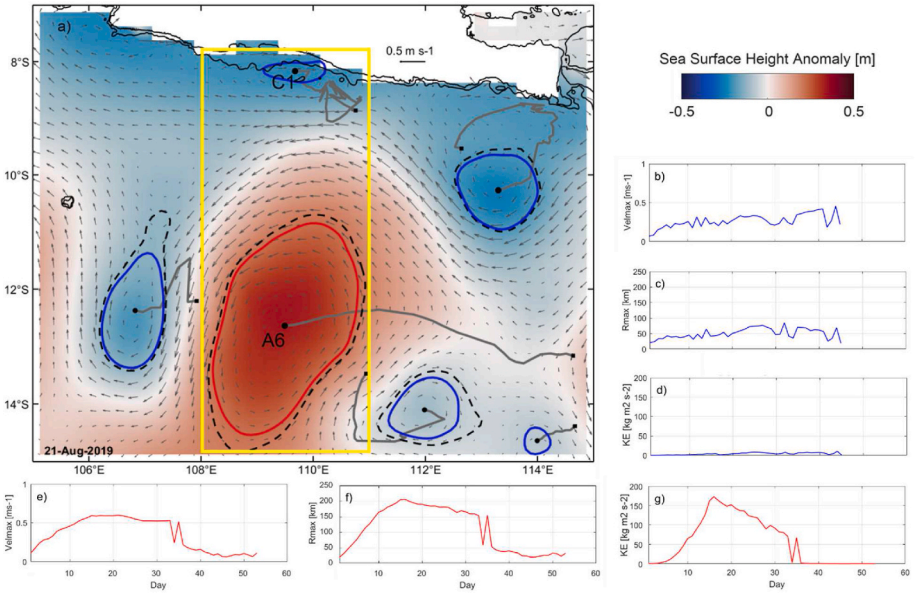

Fig. 2. (a) The screenshot of targeted eddies (yellow rectangle), which consist of the cyclonic eddies C1 (blue closed curve) on the nearshore and the anticyclonic eddies A6 (red closed curve) offshore, among other co-occurrent eddies on 21 August 2019. The corresponding properties are shown in the plot around. b-d, e-f) maximum velocity (Vel_{max}), radius (R_{max}), and Kinetic Energy (KE) for C1 and A6, respectively. Solid grey lines and vectors in (a) mark eddies track and geostrophic currents, respectively, while contour lines represent geostrophic currents and Isobath 40 m and 200 m. (For interpretation of the references to colour in this figure legend, the reader is referred to the Web version of this article.)

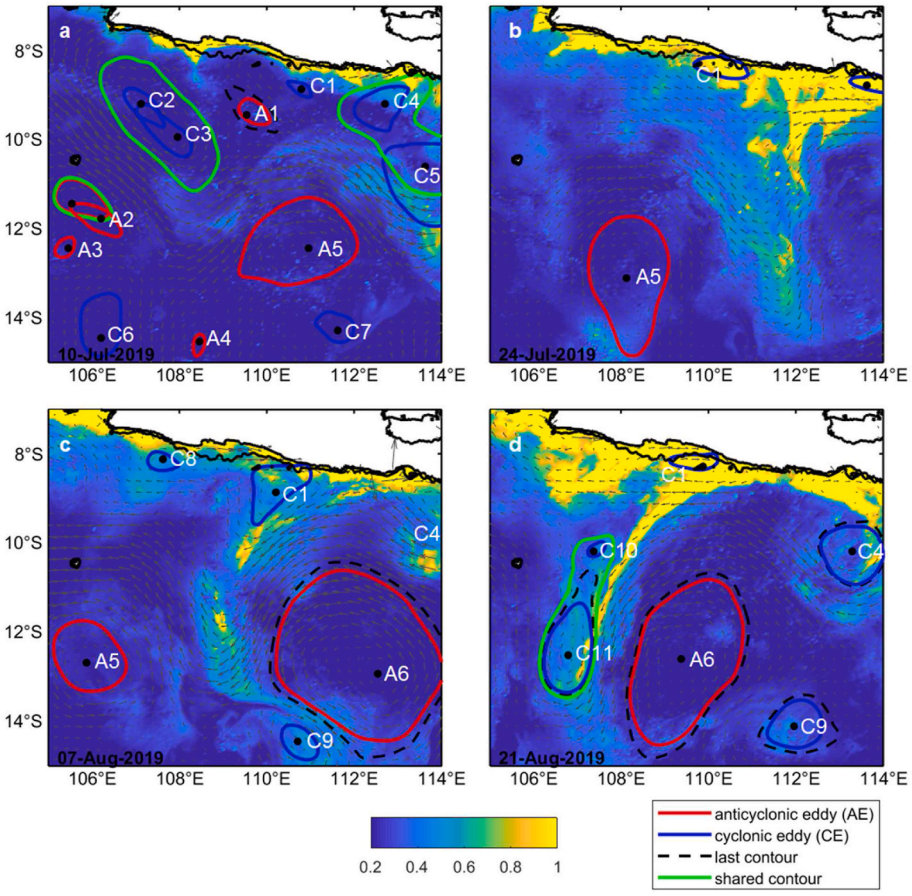

Fig. 3. Screenshots of 2 weekly upwelling filament dynamics from Chl-a (mg m^{-3}) daily chart in the study domain. The blue (red) curves represent cyclonic eddy (CE) and anticyclonic eddy (ACE), respectively. Numbered letters A and C refer to the center of ACE and CE, respectively. A vector shows a geostrophic current.C1 and A6 were selected as the targeted eddy for this study. (For interpretation of the references to colour in this figure legend, the reader is referred to the Web version of this article.)

perimeter of C8. Two weeks later, on 21 August 2019, C1 encroached on the coast, and the Chl-a filaments were still stretching up to 15° S latitude, but now with higher concentrations (0.8–1 mg m^{-3}) than before (0.5–0.8 mg m^{-3}) (Fig. 3d). The end of the filament is on the more westerly side, at position 14°S 112°E or around the perimeter of C9. C9 is at about the same latitude as before (14°S) but is now on a more easterly side than before, indicating that it is moving east until it reaches longitude 112°E. It appears that during its movement, C9 carries the filament distributed by C1, causing the ends of its filaments to be on C9's perimeter at 112°E. The presence of C9 and C10 at latitudes 10°S and 13°S, respectively, appears to play a role in distributing the filaments further south until they reach 15°S.

3.3. *Upwelling filament flux*

Using a Chl-a horizontal gradient threshold of 0.2 mg m^{-3} along the filament cross-section at 9°S on 21 August 2019, the width of the filament (w) was approximately 60.18 km (Fig. 4). The mean surface geostrophic current velocity (v) inside the eddy is about 0.3 m s^{-1}. Then, using the thickness of the jet (d) of 100 m, we estimated that the filament was transported offshore through the eddy-induced jet at rate of 1.80 Sv. Given that the mean concentration of Chl-a inside the filament is 1.3 mg m^{-3}, the total amount of Chl-a delivered offshore by this eddy is approximately 46.66 tons per day. Therefore, if this targeted eddy transports the same amount of Chl-a during its lifetime, then the total Chl-a transported offshore during the 40 days by this targeted eddy is around 1.87 × 10^3 tons.

Meanwhile, the estimated cold SST filament, which is transported

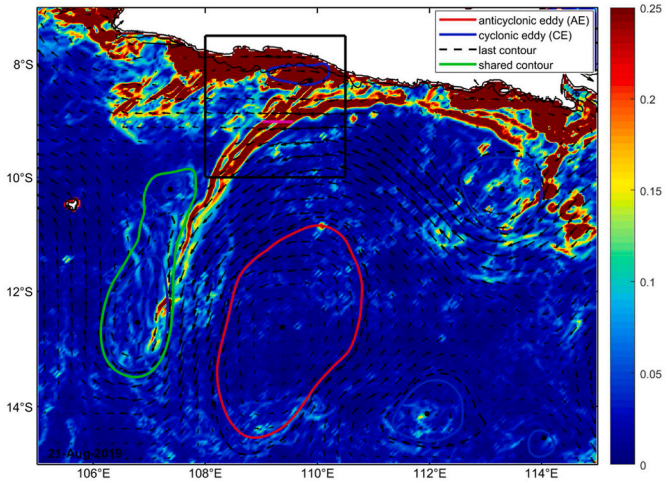

Fig. 4. The eddy-induced filament events on 21 August 2019 are used as a reference for estimating filament flux offshore. The black rectangle marks the targeted eddy (blue curve) and the filament width (magenta line) based on Chl-a with a horizontal gradient threshold of 0.2 mg km^{-1}. (For interpretation of the references to colour in this figure legend, the reader is referred to the Web version of this article.)

offshore, yielded a value of 2.33 Sv since the width of the filament has a value of 77.77 km. Using a similar variable value of mean Chl-a inside the filaments and assuming that the transport value is constant over the targeted eddy lifetimes, the amount of Chl-a transported offshore is about 60.39 tons in a day or about 2.40 $\times$ 10^3 tons in 40 days.

3.4. Wind-induced filament

The spatial distribution of chlorophyll-a (Chl-a) reveals higher concentrations in coastal waters compared to offshore areas (Fig. 5a). The upwelling processes during this period increased Chl-a values, exceeding 4 mg m^{-3} in coastal regions. Interestingly, Chl-a concentrations of 0.3–0.4 mg m^{-3} were observed far offshore, extending eastward up to 12°S and reaching 15°S along longitude 112°E, although in a patchy distribution.

Mean wind vectors predominantly show a southeasterly direction with speeds generally below 5 m s^{-1} in the eastern part, progressively increasing to over 5 m s^{-1} in the western part of the study area (Fig. 5b). A negative correlation between zonal wind stress and Chl-a indicates a direct relationship between easterly wind events and higher Chl-a concentrations. The correlation coefficient in the water area ranges from 0.6 to 1, except for regions with latitudes higher than 14°S. Notably, a stronger correlation exists offshore in the western part (0.8–1) compared to the eastern part (<0.7) (Fig. 5c). Zonal wind stress appears to have a weaker correlation at latitudes higher than 14°S.

High Chl-a concentrations occur less than five days after zonal wind stress events in coastal waters and less than ten days offshore (Fig. 5d). Similarly, meridional wind stress shows a negative correlation with Chl-a. The correlation coefficient in the water area ranges from 0.6 to 1, except for regions above 14°S. The western part has higher values (0.8–1) compared to the eastern part (<0.7) (Fig. 5e). The weakest correlation for meridional wind stress is found in the southernmost region starting from latitudes 14°S. High Chl-a concentrations occur less than five days after meridional wind stress events in coastal waters and about 10–20 days offshore (Fig. 5f).

4. Discussion

This study shows the role of two eddies in cross-shelf transport by distributing the upwelling filament containing water and materials (Chl-a and heat). South of Java tend to have a high eddy activity (Yang et al., 2015; Ismail et al., 2021). Hanifah et al. (2016) stated that shear velocity provides a good explanation for the formation of eddies in this study domain. The targeted eddies in this study can be categorized as mesoscale eddies due to their average diameter of 50 km and a lifetime of 40 days. AMEDA was used to identify and track eddies in this eddy-induced filament study. We argue that AMEDA, which uses hybrid approaches, is appropriate for this upwelling filament flux investigation because the data processing and analysis are focused on the eddy perimeter and neighboring locations. Lian et al. (2019) concluded that for a case study focusing on the peripheral area of an eddy, the WA (Windowed Angle), Sea Level Anomaly (SLA), and hybrid methods are advisable. The occurrence of the targeted eddy coincides with the south Java upwelling event, which occurs regularly during the peak of the southeast monsoon from July to August (Horii et al., 2018; Budiman et al., 2022). As a result, our intended eddy moved among the high Chl-a and low SST characteristics at that time and tended to disperse these features further offshore as filaments, as suggested by Cordeiro et al. (2015).

According to Fig. 1, a filament that can be recognized by high Chl-a and cold SST features (Clemente-Colón, 2001; Marcello et al., 2005; Smyth et al., 2001; Vipin et al., 2015) was distributed offshore, as well as those with high absolute horizontal gradients from the coastal area (7°-8°S) offshore until reaching 14°-15°S from 10 July to 25 August 2019. This condition coincides with a single frontal cyclonic eddy, C1, at the shelf area. According to Iskandar et al. (2010), offshore Chl-a blooms in the southeastern tropical Indian Ocean, particularly in the south of Java during boreal summer-fall 2006, are markedly coincident with high eddy kinetic energy. During the targeted eddies' lifetime, C1 was constantly in the near-coastal area, rich in chlorophyll due to seasonally wind-driven south Java upwelling. This condition causes the upwelling filaments to distribute offshore and accumulate there continuously.

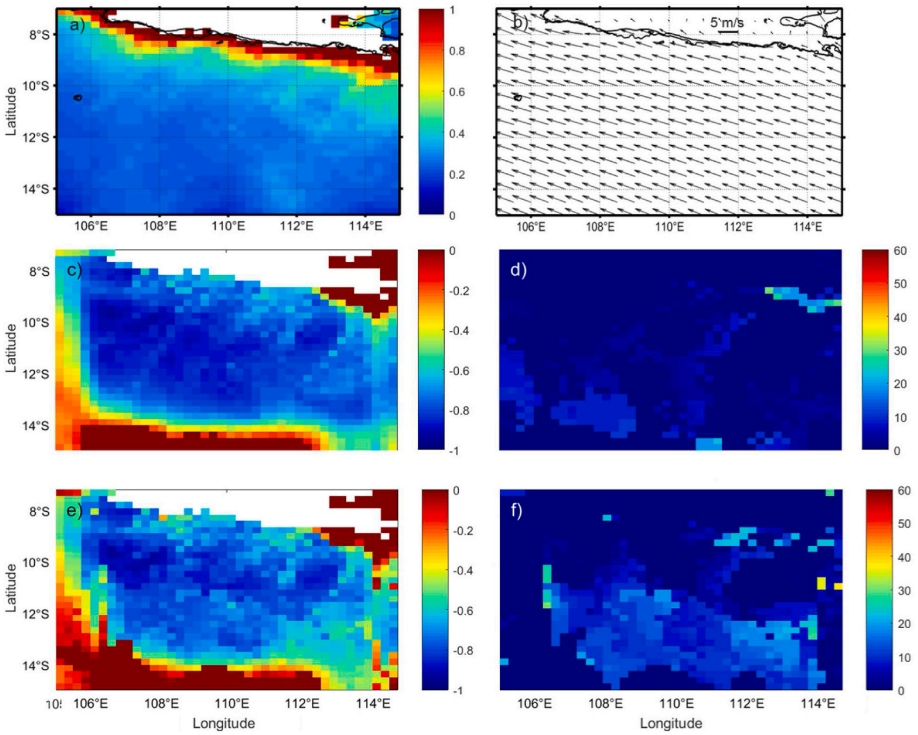

Fig. 5. The mean Chl-a in mg m^{-3} (a), wind vector in m s^{-1} (b), correlation value between zonal wind stress and Chl-a, and its corresponding lag time in days (c and d, respectively), and correlation value between meridional wind stress and Chl-a, and its corresponding lag time in days (c and d, respectively).

The peak of CE's and ACE's KE values is influenced by several factors, including their size, intensity, and the surrounding oceanographic conditions (Chelton et al., 2011). The larger eddy typically has a higher peak of KE values than the smaller one due to its large mass and energy. In turn, it has high intensity and stronger currents. For this reason, we suggest that ACE A6 is an energetic eddy that is likely to have strong currents and to be transporting water and nutrients over long distances due to its large size. This can be seen in Fig. 3c and d, which show how Chl-a filaments are distributed far south to around 15°S latitude, along with the presence of ACE A6.

This study can only estimate the transport of upwelling filaments in the top 100 m or near-surface layers due to a lack of eddy layer thickness data. Remotely sensed SST and Chl-a images only provide information about the surface characteristics of filaments, but in situ observations provide a better understanding of the vertical structure of currents and density gradients advecting filaments (Navarro-Olache et al., 2004; Shapiro et al., 2010). However, Cravo et al. (2010) stated that upper-layer structures barely exceeding the top 150 m can be considered when deciding the depth of a filament. The result of utilizing a depth of 100 m as a variable of H is that the filament flux yielded in the calculation defines the volume transport of the jet in the top 100 m, not the total mass of filaments entirely displaced by the eddies, as was obtained by (Shapiro et al., 2010) in their study. Nevertheless, the calculation results of the filament flux in this study can demonstrate the role of eddies in displacing water masses and materials from the shelf area to the offshore in the south of Java's transitional zone. The filament flux of 1.8 Sv (2.33 Sv) based on Chl-a (SST) that was obtained in this study is 6–7 times higher than that reported by Shapiro et al. (2010) with the same formula. These differences could be caused by variations in the values of the variables utilized in line with data availability and by differences in the filament width determination techniques. The comparison between the findings of this study and existing literature on eddy-induced cross-shelf transport is provided in Table 1 below.

The width of the filament based on the Chl-a and SST gradients has a difference of about 17.59 km. This value is relatively larger than that produced by Ribbe et al. (2018), who estimated the width of the filament through the maximum gradient and yielded a difference of 4 km (see Fig. 3 in Ribbe et al., 2018). Therefore, this difference is not surprising considering that Chl-a and SST are two variables with advantages and disadvantages in recognizing upwelling features. The advantage of using these variables is that they are easily accessible and can be measured remotely using satellite data. The disadvantage of using these variables is that they are not always reliable indicators of upwelling, as other processes (e.g., rainfall and river discharges) can also impact their concentrations along the coast (Navarro and Ruiz, 2006; Santos and Ribeiro, 2005). Rainfall can decrease SST and increase Chl-a due to the influx of freshwater and nutrients into the ocean (Chinacalle-Martinez et al., 2021), while river discharge influences SST and Chl-a by introducing nutrients and organic matter into the water column (Alvarez et al., 2012). Thus, the determination of upwelling based on SST and chlorophyll will produce different results. However, the impact of these processes on the filament's width based on Chl-a and SST gradients is not well understood and requires further research.

The filament upwelling flux generated in the calculations is caused by a single eddy (C1), ignoring the various influencing factors or processes mentioned above. This flux is small compared to the actual flux during the upwelling period. However, the amount of filament flux induced by the targeted eddy in this study has been able to enrich Chl-a offshore by 46.66–60.39 tons a day and could contribute to increasing biological productivity offshore, as suggested by previous studies (Iskandar et al., 2010; Ismail et al., 2021; Yang et al., 2019). Fig. 3 shows that eddies C4 and C8 transport filaments offshore even before the targeted eddy (C1) appears. An extended westward filament was formed between eddies A1, A5, C3, and C5 in latitudes 10° to 14°S (Fig. 3a). Cold subsurface water filaments that upwelled in coastal areas with favorable winds are acknowledged as effective contributors to the mechanisms that link productive coastal waters with open ocean oligotrophic waters (Levy, 2008). The development of large upwelling filaments favors horizontal offshore mass transfer (Álvarez-Salgado et al., 2001). Moreover, Cravo et al. (2010) found that the amounts of chlorophyll and nutrients transported through the filament are significant.

Table 1
The comparison between the findings of this study and the previous studies on eddy-induced cross-shelf transport.

No	Researcher	Study Domain	Filament metrics	Cross-shelf Flux	Chl-a Filament Flux
1	Peliz et al. (2004)	SW Iberia	$v = 0.15$ m s^{-1}	0.7 Sv (~58 km^3 per day) per-day	63 Tons/day
2	Shapiro et al. (2010)	NW Black Sea	$w = 30$ km $d = 150$ m $v = 0.15$ m s^{-1}	0.3 Sv per day	Not quantified
3	Ribbe et al. (2018)	East Australia	$w = 20$ km $d = 100$ m $v =$ 0.28–0.5 m s^{-1}	0.3–1.8 Sv per-day	13-78 Tons/ per-day
4	Akpinar et al. (2022)	Black sea	$w =$ 12–37.5 km $d = 100$ m $v = 0.3$ m s^{-1}	0.4 Sv per-day	Not quantified
5	This Study	South Java	$w = 11$ km $d = 130$ m $v = 0.3$ m s^{-1}	1.8 Sv per-day	46.66–60.39 Tons/day
			$w = 60.18$ km $d = 100$ m		

v, w, d are the filament's velocity, width, and thickness or depth, respectively.

The cross-correlation analysis suggests that zonal and meridional wind stress correlate significantly with Chl-a south of Java Water. However, the nature of the influence varies depending on the location. In the coastal (offshore) waters, both zonal and meridional wind stress have a higher (weaker) correlation value with Chl-a concentrations in the negative direction. This is likely because southeasterly winds promote upwelling (Horii et al., 2018; Wirasatriya et al., 2020; Budiman et al., 2022), which brings nutrient-rich subsurface waters to the surface and leads to increased Chl-a concentrations. The lag of 4 (6) days between the peak of zonal (meridional) wind stress and the peak of Chl-a concentrations suggests that it takes some time for the upwelled nutrients to be assimilated by phytoplankton and for chlorophyll-a concentrations to respond (Budiman et al., 2022), and takes about 10–12 days for the advective transport of chlorophyll-rich surface waters offshore.

According to the analysis result, we proposed three forces involved in Chl-a distribution in our study domain: winds, the frontal cyclonic eddy onshore, and the anticyclonic eddy offshore. There are at least three stages to explain the presence of nutrient-rich coastal waters offshore: wind-induced upwelling, as shown in previous studies (Horii et al., 2018; Wirasatriya et al., 2020; Budiman et al., 2022), the retention and offshore export by frontal cyclonic eddy onshore, and the advection further south by anticyclonic eddy offshore. Our analysis shows that wind also significantly correlates with Chl-a in offshore areas, indicating

that the Chl-advection process in waters cannot ignore the role of wind.

It should be noted that the filament upwelling flux produced in the calculations is the sum of the flux generated by one cyclonic eddy C1 assisted by anti-cyclonic A6 and the wind that distributes this flux further offshore. This flux is small compared to the actual flux during the upwelling period. However, the amount of filament flux induced by the targeted eddy in this study has been able to enrich Chl-a offshore by 46.66–60.39 tons a day and could contribute to increasing biological productivity offshore, as suggested by previous studies (Iskandar et al., 2010; Ismail et al., 2021; Yang et al., 2019). Fig. 3 shows that eddy C4 and C8 transport filament offshore, even before the targeted eddy (C1) appears. An extended westward filament was formed between eddies A1, A5, C3, and C5 in latitudes 10° to 14°S (Fig. 3a). Cold subsurface water filaments that upwelled in coastal areas with favorable winds are acknowledged as effective contributors to the mechanisms that link productive coastal waters with open ocean oligotrophic waters (Levy, 2008). The development of large upwelling filaments favors horizontal offshore mass transfer (Álvarez-Salgado et al., 2001). Moreover, Cravo et al. (2010) found that the amounts of chlorophyll and nutrients transported through the filament are significant.

This study uses remotely sensed data. An in-situ current measurement inside the eddy perimeter is preferable for better water flux analysis and results. A limitation is that satellites can only see the surface layer of the oceans.

5. Conclusions

This study reveals the significant role of mesoscale eddies in transporting upwelled water and associated materials (Chl-a and heat) offshore on the southern Java coast. We suggest a three-stage mechanism to explain this: wind-driven upwelling intensifying coastal nutrients, the retention and offshore export by frontal cyclonic eddy onshore, and the advection further south by anticyclonic eddy offshore. This research sheds light on the spatial distribution of nutrients and primary productivity in this region, highlighting the importance of eddies in ocean circulation and biogeochemical processes. The targeted cyclonic eddy traveled for 45 days from 10 July to 25 August 2019 near the shelf area, while the targeted anticyclonic eddy propagated for 53 days from 22 July 2019 to 13 September 2019. These eddies distributed the high Chl-a and cold SST offshore in filament forms. We used the Chl-a and SST daily charts on 21 August 2019 to determine the filament flux. We used the formula from previous studies to estimate the upwelling filament flux in the top 100 m. However, this depth only limits the amount of filament transported, and there are limitations to this formula. However, the filament flux generated in the calculation is large enough to enrich Chl-a offshore and could contribute to increasing biological productivity there.

A three-stage mechanism causes the occurrence of nutrient-rich coastal waters offshore. Initially, southeasterly winds generated coastal upwelling, bringing nutrient-rich subsurface waters to the surface and elevated chlorophyll-a (Chl-a) concentrations in coastal waters. Subsequently, the formation of eddy C1 at the shelf area facilitated the transport of these upwelling-enriched waters offshore. Once displaced, eddy A1 helped continue the distribution and advect these nutrient-rich waters further offshore. Meanwhile, anticyclonic A6 distributed Chl-a further south on the 13th day of C1 propagation. Thus, the combination of enhanced coastal upwelling driven by southeasterly winds and the distribution and retention capabilities of eddy C1 and A6 can explain nutrient-rich coastal waters in offshore regions.

Future research could focus on the long-term impact of eddy-induced transport, investigating its influence on regional biogeochemical cycles over time. Additionally, quantifying the role of different eddy types and their interactions in cross-shelf exchanges would be valuable. Developing coupled physical-biogeochemical models and exploring the connectivity between upwelling systems and downstream ecosystems are further promising avenues for research. By addressing these directions, we can better understand the complex interactions governing this system, leading to improved predictions and sustainable management of marine resources.

CRediT authorship contribution statement

Mochamad Furqon Azis Ismail: Methodology, Writing – review & editing, Supervision, Validation, Conceptualization, Writing – original draft. **Asep Sandra Budiman:** Conceptualization, Data curation, Formal analysis, Investigation, Methodology, Visualization, Writing – original draft, Writing – review & editing. **Abdul Basit:** Writing – review & editing. **Erma Yulihastin:** Conceptualization, Formal analysis, Visualization, Writing – review & editing. **Iis Sofiati:** Writing – review & editing, Writing – original draft. **Subekti Mujiasih:** Writing – original draft, Writing – review & editing.

Declaration of generative AI and AI-assisted technologies in the writing process

During the preparation of this work the author(s) used microsoft Bing AI in order to improve language and readability. After using this tool/service, the author(s) reviewed and edited the content as needed and take(s) full responsibility for the content of the publication.

Declaration of competing interest

The authors declare the following financial interests/personal relationships which may be considered as potential competing interests: MFAI reports financial support was provided by GEOMAR Helmholtz Centre for Ocean Research Kiel. ASB reports financial support was provided by Research Organization of Electronics and Informatics, The National Research and Innovation Agency, Indonesia. If there are other authors, they declare that they have no known competing financial interests or personal relationships that could have appeared to influence the work reported in this paper.

Acknowledgements

We acknowledge the E.U. Copernicus Marine Service Information that provided satellite data. MFAI acknowledges funding support from the Georg Foster Research Fellowship of the Alexander von Humboldt and GEOMAR Helmholtz Centre for Ocean Research Kiel. ASB acknowledges funding support from the Research Organization of Electronics and Informatics - The National Research and Innovation Agency, Indonesia under the Program House of a Decision Support System Prototype based on Satellite Image Analysis batch II.

References

Akpinar, A., Sadighrad, E., Fach, B.A., Arkın, S., 2022. Eddy induced cross-shelf exchanges in the black sea. Rem. Sens. 14 (19) https://doi.org/10.3390/rs14194881.

Álvarez-Salgado, X.A., Doval, M.D., Borges, A.V., Joint, I., Frankignoulle, M., Woodward, E.M.S., Figueiras, F.G., 2001. Off-shelf fluxes of labile materials by an upwelling filament in the nw iberian upwelling system. Prog. Oceanogr. 51 (2–4), 321–337. https://doi.org/10.1016/S0079-6611(01)00073-8.

Alvarez, I., Lorenzo, M.N., deCastro, M., 2012. Analysis of chlorophyll a concentration along the Galician coast: seasonal variability and trends. ICES (Int. Counc. Explor. Sea) J. Mar. Sci. 69 (5), 728–738. https://doi.org/10.1093/icesjms/fss045. July 2012.

Artal, O., Sepúlveda, H.H., Mery, D., Pieringer, C., 2018. Detecting and characterizing upwelling filaments in a numerical ocean model. Comput. Geosci. 122 (September 2018), 25–34. https://doi.org/10.1016/j.cageo.2018.10.005.

Barbieri, M.A.B., Bravo, M.R., Farías, M.S., Ciencias, E. De., 1995. Fenómenos asociados a la estructura térmica superficial del mar observados a través de imágenes satelitales en la zona norte de Chile. Invest. Mar., Valparaíso 23, 99–122.

Bassin, C.J., Washburn, L., Mcphee-shaw, E., 2005. Sub-mesoscale coastal eddies observed by high frequency radar : a new mechanism for delivering nutrients to kelp forests in the Southern California Bight. Geophys. Res. Lett. 32, L12604 https://doi.org/10.1029/2005GL023017, 10.1029/2005GL023017, 200532(v), 1–4.

Budiman, A.S., Bengen, D.G., Nurjaya, I.W., Arifin, Z., Ismail, M.F.A., 2022. A comparison of the three upwelling indices in the South Java sea shelf. CMU J. Nat. Sci. 21 (3), e2022044 https://doi.org/10.12982/CMUJNS.2022.044.

Chelton, D.B., Schlax, M.G., Samelson, R.M., 2011. Progress in Oceanography Global observations of nonlinear mesoscale eddies. Prog. Oceanogr. 91 (2), 167–216. https://doi.org/10.1016/j.pocean.2011.01.002.

Chinacalle-Martínez, N., García-Rada, E., López-Macías, J., Pinoargote, S., Loor, G., Zevallos-Rosado, J., Cruz, P., Pablo, D., Andrade, B., Robalino-Mejía, C., Añazco, S., Guerrero, J., Intriago, A., Veelenturf, C., Peñaherrera-Palma, C., 2021. Oceanic primary production trend patterns along coast of Ecuador. Neotropical Biodiversity 7 (1), 379–391. https://doi.org/10.1080/23766808.2021.1964915.

Clemente-Colón, 2001. Evolution of upwelling-associated biological features in the middle Atlantic Bight as Captured by SAR , SST , and ocean color Sensors. IGARSS 2001. Scanning the present and Resolving the Future. Proceedings. IEEE 2001 International Geoscience and Remote Sensing Symposium (Cat. No.01CH37217), pp. 2616–2618. https://doi.org/10.1109/IGARSS.2001.978107.

Cordeiro, N.G.F., Nolasco, R., Cordeiro-Pires, A., Barton, E.D., Dubert, J., 2015. Journal of Geophysical research : oceans filaments on the western iberian margin : a modeling study. J. Geophys. Res. Oceans 120, 5400–5416. https://doi.org/10.1002/2014JC010688.

Cravo, A., Relvas, P., Cardeira, S., Rita, F., Madureira, M., Sa, R., 2010. An upwelling filament off southwest Iberia : Effect on the chlorophyll a and nutrient export. Continent. Shelf Res. 30 (2010), 1601–1613. https://doi.org/10.1016/j.csr.2010.06.007.

Feng, M., Wijffels, S., 2002. Intraseasonal variability in the South Equatorial current of the east Indian ocean. Phys. Oceanogr. 32, 265–277.

García-Muñoz, M., Arístegui, J., Montero, M.F., Barton, E.D., 2004. Distribution and transport of organic matter along a filament-eddy system in the Canaries - NW Africa coastal transition zone region. Prog. Oceanogr. 62 (2–4), 115–129. https://doi.org/10.1016/j.pocean.2004.07.005.

Hanifah, F., Ningsih, N.S., Sofian, I., 2016. Dynamics of eddies in the southeastern tropical Indian ocean dynamics of eddies in the southeastern tropical Indian ocean. J. Phys.: Conf. Ser. 739, 012042 https://doi.org/10.1088/1742-6596/739/1/012042.

Harrison, C.S., Siegel, D.A., Mitarai, S., 2013. Filamentation and eddy-eddy interactions in marine larval accumulation and transport. Mar. Ecol. Prog. Ser. 472, 27–44. https://doi.org/10.3354/meps10061.

Hatmaja, R.B., Ramadhan, M.R., Wicaksana, S.K.J., Suaydhi, 2023. Anomalous Sea surface temperature and chlorophyll-a induced by mesoscale cyclonic eddies in the southeastern tropical Indian Ocean during the 2019 Extreme positive Indian Ocean Dipole. In: Proceedings of the International Conference on Radioscience, Equatorial Atmospheric Science and Environment and Humanosphere Science. INCREASE 2022. Springer Proceedings in Physics, vol. 290. Springer, Singapore. https://doi.org/10.1007/978-981-19-9768-6_47.

Horii, T., Ueki, I., Ando, K., 2018. Coastal upwelling events along the southern coast of Java during the 2008 positive Indian Ocean Dipole. J. Oceanogr. 1999 https://doi.org/10.1007/s10872-018-0475-z.

Iskandar, I., Sasaki, H., Sasai, Y., Masumoto, Y., Mizuno, K., 2010. A numerical investigation of eddy-induced chlorophyll bloom in the southeastern tropical Indian Ocean during Indian Ocean Dipole - 2006. Ocean Dynam. 60 (3), 731–742. https://doi.org/10.1007/s10236-010-0290-6.

Ismail, M.F.A., Ribbe, J., Karstensen, J., Lemckert, C., Lee, S., Gustafson, J., 2017. The Fraser Gyre : a cyclonic eddy off the coast of eastern Australia. Estuar. Coast Shelf Sci. 192, 72–85. https://doi.org/10.1016/j.ecss.2017.04.031.

Ismail, M.F.A., Ribbe, J., Arifin, T., Taofiqurohman, A., Anggoro, D., 2021. A census of eddies in the tropical eastern boundary of the Indian Ocean. J. Geophys. Res.: Oceans (n/a), e2021JC017204. https://doi.org/10.1029/2021JC017204 n/a.

Jiaxun, Li., Wang, G., Zhai, X., 2017. Observed cold filaments associated with mesoscale eddies in the South China Sea. J. Geophys. Res.: Oceans RESEARCH 762–770. https://doi.org/10.1002/2016JC012353.

Le Vu, B., Stegner, A., Arsouze, T., 2018. Angular momentum eddy detection and tracking algorithm (AMEDA) and its application to coastal eddy formation. J. Atmos. Ocean. Technol. 35 (4), 739–762. https://doi.org/10.1175/JTECH-D-17-0010.1.

Levy, M., 2008. The Modulation of biological production by oceanic mesoscale Turbulence. Lect. Notes Phys. 744, 219–261. https://doi.org/10.1007/978-3-540-75215-8, 10.1007/978-3-540-75215-8 9 (Vol. 261).

Lian, Z., Sun, B., Wei, Z., Wang, Y., Wang, X., 2019. Comparison of eight detection algorithms for the quantification and characterization of mesoscale eddies in the South China Sea. J. Atmos. Ocean. Technol. 36 (7), 1361–1380. https://doi.org/10.1175/JTECH-D-18-0201.1.

Lumban-Gaol, J., Siswanto, E., Mahapatra, K., Natih, N.M.N., Nurjaya, I.W., Hartanto, M. T., Maulana, E., Adrianto, L., Rachman, H.A., Osawa, T., Rahman, B.M.K., Permana, A., 2021. Impact of the strong downwelling (Upwelling) on small pelagic fish production during the 2016 (2019) negative (positive) indian ocean dipole events in the eastern indian ocean off java. Climate 9 (2), 1–11. https://doi.org/10.3390/cli9020029.

Marcello, J., Marqués, F., Eugenio, F., Member, A., 2005. Automatic tool for the Precise detection of upwelling and filaments in remote sensing Imagery. IEEE Trans. Geosci. Rem. Sens. 43 (7), 1605–1616. https://doi.org/10.1109/TGRS.2005.848409.

McGillicuddy, D.J., 2016. Mechanisms of physical-biological-biogeochemical interaction at the oceanic mesoscale. Ann. Rev. Mar. Sci 8 (Issue September 2015). https://doi.org/10.1146/annurev-marine-010814-015606.

Navarro-olache, L.F., Lavı, M.F., Alvarez-sa, L.G., Zirino, A., 2004. Internal structure of SST features in the central Gulf of California. Deep-Sea Research II 51 (673–687 51), 673–687. https://doi.org/10.1016/j.dsr2.2004.05.014, 2004.

Navarro, G., Ruiz, J., 2006. Spatial and temporal variability of phytoplankton in the Gulf of Cadiz through remote sensing images. Deep-Sea Research II 53, 1241–1260. https://doi.org/10.1016/j.dsr2.2006.04.014.

Peliz, Á., Santos, A.M.P., Oliveira, P.B., Dubert, J., 2004. Extreme cross-shelf transport induced by eddy interactions southwest of Iberia in winter 2001. Geophys. Res. Lett. 31 (8), 2–5. https://doi.org/10.1029/2004GL019618.

Pessini, F., Olita, A., Cotroneo, Y., Perilli, A., Oristano, C.N.R., 2018. Mesoscale eddies in the Algerian Basin : do they differ as a function of their formation site. Ocean Sci. 14, 669–688. https://doi.org/10.5194/os-14-669-2018, 2018.

Ribbe, J., Toaspern, L., Wolff, J.-O., Ismail, M.F.A., 2018. Frontal eddies along a western boundary current. Continent. Shelf Res. 165, 51–59. https://doi.org/10.1016/j.csr.2018.06.007.

Rodriguez, Herna, S., Barton, E.D., 1999. Mesoscale distribution of fish larvae in relation to an upwelling filament of Northwest Africa. Deep-Sea Res. I 46 (1999), 1969–1984.

Rubio, A., Caballero, A., Orfila, A., Hernández-Carrasco, I., Ferrer, L., González, M., Solabarrieta, L., Mader, J., 2018. Eddy-induced cross-shelf export of high Chl-a coastal waters in the SE Bay of Biscay. Rem. Sens. Environ. 205 (March 2017), 290–304. https://doi.org/10.1016/j.rse.2017.10.037.

Santos, A.M.P., Ribeiro, A.C., 2005. A study of the response of chlorophyll- a biomass to a winter upwelling event off Western Iberia using SeaWiFS and in situ data. J. Mar. Syst. 53, 87–107. https://doi.org/10.1016/j.jmarsys.2004.05.031.

Shapiro, G.I., Stanichny, S.V., Stanychna, R.R., 2010. Anatomy of shelf-deep sea exchanges by a mesoscale eddy in the North West Black Sea as derived from remotely sensed data. Rem. Sens. Environ. 114 (4), 867–875. https://doi.org/10.1016/j.rse.2009.11.020.

Smyth, T.J., Miller, P.I., Groom, S.B., Lavender, S.J., 2001. Remote sensing of sea surface temperature and chlorophyll during Lagrangian experiments at the Iberian margin. Prog. Oceanogr. 51 (2–4), 269–281. https://doi.org/10.1016/S0079-6611(01)00070-2.

Vazquez-cuervo, J., Torres, H.S., Menemenlis, D., Chin, T., Armstrong, E.M., Torres, H.S., Menemenlis, D., Chin, T., Vazquez-cuervo, J., Torres, H.S., Menemenlis, D., Chin, T., Armstrong, E.M., 2017. Relationship between SST gradients and upwelling off Peru and Chile : model/satellite data analysis Relationship between SST gradients and upwelling off Peru. Int. J. Rem. Sens. 38 (23), 6599–6622. https://doi.org/10.1080/01431161.2017.1362130.

Vipin, P., Sarkar, K., Aparna, S.G., Shankar, D., Sarma, V.V.S.S., Gracias, D.G., Krishna, M.S., Srikanth, G., Mandal, R., Rao, E.P.R., Rao, N.S., 2015. Evolution and sub-surface characteristics of a sea-surface temperature filament and front in the northeastern Arabian Sea during November–December 2012. J. Mar. Syst. https://doi.org/10.1016/j.jmarsys.2015.05.003. December 2012.

Wirasatriya, A., Setiawan, J.D., Sugianto, D.N., Rosyadi, I.A., Haryadi, H., Winarso, G., Setiawan, R.Y., Susanto, R.D., 2020. Ekman dynamics variability along the southern coast of Java revealed by satellite data. Int. J. Rem. Sens. 41 (21), 8475–8496. https://doi.org/10.1080/01431161.2020.1797215.

Yang, G., Yu, W., Yuan, Y., Zhao, X., Wang, F., Chen, G., Liu, L., Duan, Y., 2015. Characteristics, vertical structures, and heat/salt transports of mesoscale eddies in the southeastern tropical Indian Ocean. J. Geophys. Res. Oceans 6733–6750. https://doi.org/10.1002/2015JC011130.

Yang, G., Zhao, X., Li, Y., Liu, L., Wang, F., Yu, W., 2019. Chlorophyll variability induced by mesoscale eddies in the southeastern tropical Indian Ocean. J. Mar. Syst. 199 (September 2018), 103209 https://doi.org/10.1016/j.jmarsys.2019.103209.

Yu, Z., Potemra, J., 2006. Generation mechanism for the intraseasonal variability in the Indo-Australian basin. J. Geophys. Res.: Oceans 111 (1), 1–11. https://doi.org/10.1029/2005JC003023.